

# Extending a serial 3D two-phase CFD code to parallel execution over MPI by using the PETSc library for domain decomposition

Åsmund Ervik, Svend Tollak Munkejord and Bernhard Müller

15th October 2018

This paper has been submitted to the CFD 2014 conference.

## Abstract

To leverage the last two decades' transition in High-Performance Computing (HPC) towards clusters of compute nodes bound together with fast interconnects, a modern scalable CFD code must be able to efficiently distribute work amongst several nodes using the Message Passing Interface (MPI). MPI can enable very large simulations running on very large clusters, but it is necessary that the bulk of the CFD code be written with MPI in mind, an obstacle to parallelizing an existing serial code.

In this work we present the results of extending an existing two-phase 3D Navier-Stokes solver, which was completely serial, to a parallel execution model using MPI. The 3D Navier-Stokes equations for two immiscible incompressible fluids are solved by the continuum surface force method, while the location of the interface is determined by the level-set method.

We employ the Portable Extensible Toolkit for Scientific Computing (PETSc) for domain decomposition (DD) in a framework where only a fraction of the code needs to be altered. We study the strong and weak scaling of the resulting code. Cases are studied that are relevant to the fundamental understanding of oil/water separation in electrocoalescers.

## Nomenclature

$\mu$	Dynamic viscosity of a fluid.	Pa·s
$\nu$	Kinematic viscosity of a fluid.	m <sup>2</sup> /s
$\rho$	Density of a fluid.	kg/m <sup>3</sup>
$\mathbf{f}$	External acceleration.	m/s <sup>2</sup>
$\mathbf{u}(\mathbf{x})$	Velocity field of a fluid.	m/s
$p(\mathbf{x})$	Pressure of a fluid.	Pa
$\kappa$	Curvature of the interface.	1/m
$\sigma$	Coefficient of surface tension.	N/m
$n$	Time step index.	
Re	Reynolds number.	

## 1 Introduction

In 1965 Gordon Moore famously predicted that transistor density (and hence computing power for a given chip) would double each year in the foreseeable future Moore (1965). Dubbed Moore's law, this trend continued to hold for roughly 40 years and meant that life was easy

for people needing greater and greater computational power. While serious High-Performance Computing (HPC) was dominated in most of this period by vector machines like the seminal Cray 1, by the mid-1990s clusters of many interconnected scalar CPUs had become a cheaper solution, leading to the industry-wide adoption of distributed memory architectures.

Around 2005 Moore's law finally started hitting a barrier when the high heat production of chips and, somewhat later, the diffraction limits for photolithography began forcing chip makers to alter their ways. Two complementary solutions were introduced, namely shared-memory architectures (multi-core CPUs) and vector instruction sets (SSE, AVX, FMA)<sup>1</sup>. Both solutions were adopted in HPC, leading to hybrid shared-memory/distributed-memory systems. In the last five years accelerator technologies (GPGPU, MIC)<sup>2</sup> have furthered the return to vector processing, so HPC has in a sense come full circle. All in all this gives a very heterogeneous environment for HPC where the onus is on the application programmer to ensure that his/her code can make the most of the available resources.

In contemporary numerical codes, omitting here the use of accelerators, the two main programming paradigms for leveraging parallelism are OpenMP and MPI. OpenMP takes advantage of shared-memory architectures, while MPI can use distributed-memory architectures. On current systems, OpenMP can scale from 1 to 32 cores, while MPI can scale to thousands and even millions of cores. This means that MPI is the paradigm of choice for HPC, possibly in combination with OpenMP used by each MPI process.

We will use the following nomenclature when discussing parallelism: a "process" is one MPI rank which is executing code. A CPU has several "cores", each of which may execute a process. The CPUs are located on "nodes", e.g. a desktop computer or a blade in a cluster. Typical cluster nodes have 2 (or more) CPUs, each having a separate "socket" connecting the CPU to the memory (RAM). Each socket has one communication channel to memory shared by all cores on this socket. Many nodes can communicate over the "interconnect", which should preferably be very fast and have very low latency.

This paper will focus on the use of MPI to port an

<sup>1</sup>SSE: Streaming SIMD Extensions. AVX: Advanced Vector Extensions. FMA: Fused Multiply-Add.

<sup>2</sup>GPGPU: General-Purpose Graphics Processing Unit. MIC: Many Integrated Core.

existing serial implementation of a 2D/3D incompressible Navier-Stokes solver. This code can simulate two-phase flows relevant e.g. for the fundamental understanding of oil/water separation, but for 3D cases the runtime is very long (weeks and months). The majority of this runtime is due to the solution of a Poisson equation for the pressure, and state of the art algorithms for this problem are bound by the memory bandwidth rather than CPU speed. This makes OpenMP a poor solution in this case and leaves MPI as the necessary paradigm for parallelism. We will employ the PETSc library, specifically the DMDA component, to do domain decomposition. The solution of the Poisson equation is also done using PETSc routines. We establish a framework in Fortran where it is possible to reuse the existing serial code.

The rest of this paper is organized as follows: in the next section, the basic equations are established, after which the numerical methods are presented. Then we describe the framework and the specific changes that were needed to port the serial code. Computations performed with the resulting code are discussed and we study the strong and weak scaling on several architectures. Finally some closing remarks are given.

## 2 Model Description

The equations that govern the two-phase flow system under consideration are the incompressible Navier-Stokes equations:

$$\nabla \cdot \mathbf{u} = 0 \quad (1)$$

$$\frac{\partial \mathbf{u}}{\partial t} + (\mathbf{u} \cdot \nabla) \mathbf{u} = -\frac{\nabla p}{\rho} + \frac{\mu}{\rho} \nabla^2 \mathbf{u} + \mathbf{f} \quad (2)$$

These equations are valid for single-phase flow. To extend this formulation to two-phase flow we keep these equations in each of the two phases, where the densities and viscosities are constant in each phase. We will restrict ourselves to laminar flow, as we are interested in situations with Reynolds numbers  $\text{Re} \sim \mathcal{O}(1)$ .

Across the interface between the fluids, a jump in the normal component of the traction vector will arise due to the surface tension  $\sigma$ , and this jump together with effects of the jump in density and viscosity must be added to our equations. We introduce these effects using the continuum surface force method (CSF) Brackbill *et al.* (1992). The location of the interface is captured using the level-set method (LSM) Osher and Sethian (1988); Osher and Fedkiw (2001), see Ervik *et al.* (2014) for a detailed description, we provide only a short outline here.

The level-set method is a method for capturing the location of an interface. It is widely used not just for multi-phase fluid flow but also in other contexts where an interface separates two regions. The interface is represented by a level-set function  $\phi(\mathbf{x})$  which is equal to the signed distance to the interface. In other words, the interface is given by the zero level set  $\{\mathbf{x} \mid \phi(\mathbf{x}) = 0\}$ , hence the name. Rather than advecting the interface location, one advects the function  $\phi(\mathbf{x})$  directly according

to the transport equation

$$\frac{\partial \phi}{\partial t} = -\mathbf{u} \cdot \nabla \phi \quad (3)$$

giving an implicit formulation that automatically handles changes in interface topology.

The level-set method can be visualized as in Fig. 1 for a 2D fluid flow with a drop next to a film, seen on the right-hand side in this figure as gray shapes. The distance is shown as isocontour lines superimposed on these shapes. On the left-hand side the level-set function is shown visualized in 3D as surfaces where the height above water corresponds to the signed distance. The analogy to a map describing an island rising out of the water is quite striking, except that the roles of “reality” and “tool for description” have been reversed.

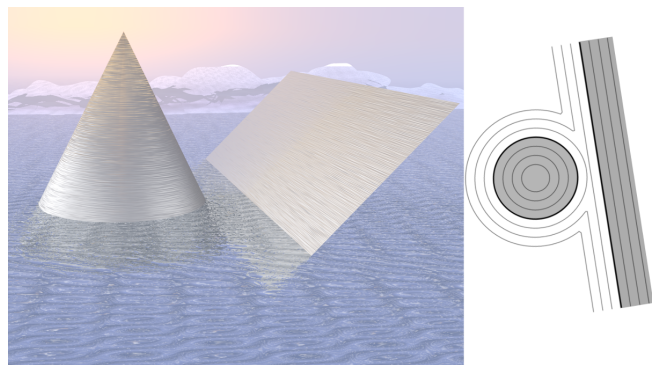


Figure 1: Illustration of the level-set method. Right: in 2D, a fluid drop (dark gray) seen next to a fluid film (dark gray), both immersed in a different fluid (white). Left: the signed-distance function representing these two fluid bodies, the drop and the film.

When the location of the interface is known, the curvature  $\kappa$  can be calculated from  $\phi$ , and together with  $\sigma$  this gives the surface tension force. In the CSF method this force is incorporated as a volume-force term which is non-zero only in a thin band around the interface. This thin band is produced by smearing out the delta function, making the force term continuous. For such a smeared-out delta function, we can compute the volume-force term at a point  $\mathbf{x}$  close to the interface as

$$\mathbf{f}_s(\mathbf{x}, t) = \int_{\Gamma} \mathbf{f}_{\text{sfd}}(s, t) \delta(\mathbf{x} - \mathbf{x}_I(s)) ds, \quad (4)$$

where  $\mathbf{f}_{\text{sfd}}$  is a surface-force density and  $\mathbf{x}_I(s)$  is a parametrization of the interface. The surface-force density is such that the integral of  $\mathbf{f}_s(\mathbf{x}, t)$  across the (smeared-out) interface approximates the surface tension force, see Brackbill *et al.* (1992) for details. Note that in the level-set context it is not necessary to parametrize the interface since  $\phi(\mathbf{x})$  stores the distance to the interface, so we have  $\mathbf{x} - \mathbf{x}_I(s) = \phi(\mathbf{x})$  as long as  $\phi(\mathbf{x})$  is a signed distance function. There are several ways to smear out the delta function, we follow Osher and Fedkiw (2003, Eq. 1.23),

$$\delta(x) = \begin{cases} 0 & \text{if } |\phi| > \epsilon \\ \frac{1}{2\epsilon} \left( 1 + \cos\left(\frac{\pi\phi}{\epsilon}\right) \right) & \text{else} \end{cases} \quad (5)$$

where  $\epsilon = 1.5\Delta x$  is employed. This one-dimensional delta function is composed into the three-dimensional version by taking  $\delta(\mathbf{x}) = \delta(x)\delta(y)\delta(z)$ .

This formulation leads to a source term which incorporates the effects of surface tension. It is also necessary to smear out the viscosity and density differences across the interface in order to be consistent with the above formulation. A smeared-out Heaviside function  $H(\mathbf{x})$  is used to accomplish this, given by Osher and Fedkiw (2003, Eq. 1.22) as

$$H(x) = \begin{cases} 0 & \text{if } \phi < -\epsilon \\ \frac{1}{2} \left( 1 + \frac{\phi}{\epsilon} + \frac{1}{\pi} \sin\left(\frac{\pi\phi}{\epsilon}\right) \right) & \text{if } -\epsilon < \phi < \epsilon \\ 1 & \text{if } \phi > \epsilon \end{cases} \quad (6)$$

### 3 Numerical methods

To discretize the Navier-Stokes equations and the equations for the level-set method we employ finite difference methods, specifically WENO Liu *et al.* (1994) for the convective terms and central differences for the viscous terms in Eq. (2), and WENO also for Eq. (3). The time integration is done with an explicit second-order Runge-Kutta method (SSPRK (2,2) in the terminology of Gottlieb *et al.* (2009)) for both Eq. (2) and Eq. (3). The grid is a structured rectangular uniform staggered grid. A staggered grid is employed to avoid checkerboarding of the pressure field; this means that the pressure and other scalars “live” at cell centers, while the velocities “live” at the cell faces. To be more precise, if we have a pressure at one point  $p_{i,j,k}$ , the velocities  $(u, v, w)$  around this point are  $u_{i\pm 1/2,j,k}, v_{i,j\pm 1/2,k}, w_{i,j,k\pm 1/2}$  located at the 6 cell faces. In the actual code we store the velocity values for  $u_{i+1/2,j,k}, v_{i,j+1/2,k}, w_{i,j,k+1/2}$  at the index  $(i, j, k)$  even though these values are not physically colocated.

The major problem when solving Eqs. (1) and (2) is that this is not a set of PDEs, it is a differential-algebraic equation (DAE) with a Hessenberg index of two. In other words, even though we have four equations (Eq. (2) is three equations) and four unknowns  $(u, v, w, p)$ , Eq. (1) cannot be used directly to find  $p$ . The first solution to this conundrum was presented by Chorin (1968). This method can be understood as calculating an approximate velocity field  $\mathbf{u}^*$  which does not satisfy Eq. (1), and subsequently projecting this velocity field onto the manifold of vector fields satisfying Eq. (1). For this reason, the method is often called Chorin’s projection method or simply *the* projection method. It consists of these three steps, where we calculate three quantities successively, namely  $\mathbf{u}^*, p_{n+1}, \mathbf{u}_{n+1}$ :

$$\frac{\mathbf{u}^* - \mathbf{u}_n}{\Delta t} = -(\mathbf{u}_n \cdot \nabla) \mathbf{u}_n + \nu \nabla^2 \mathbf{u}_n \quad (7)$$

$$\nabla^2 p_{n+1} = \frac{\rho}{\Delta t} \nabla \cdot \mathbf{u}^* \quad (8)$$

$$\mathbf{u}_{n+1} = \mathbf{u}^* - \frac{\Delta t}{\rho} \nabla p_{n+1} \quad (9)$$

The pressure Poisson equation (8) that arises here is elliptic, so the numerical solution is very time consuming and a vast amount of research has gone into developing fast solvers. For two-phase flows with high density differences, the condition number of the matrix that results when Eq. (8) is discretized will make matters even worse than for the single-phase problem Duffy *et al.* (2002). This matrix is very large even in sparse storage formats, for a  $256^3$  grid it has 117 million non-zero elements. The current state-of-the-art consists in combining a (geometric or algebraic) multigrid preconditioner with a conjugate gradient method (often BiCGStab) for solving the resulting sparse linear system. Our experience with 2D axisymmetric simulations suggests that the Bi-Conjugate Gradient Stabilized method van der Vorst (1992) with the BoomerAMG preconditioner Henson and Yang (2000) is an optimal choice. For the simulations performed here, however, the straight-forward successive over-relaxation (SOR) preconditioner turned out to be faster than BoomerAMG. This has not been investigated in greater detail. We employ the PETSc and Hypr libraries for these methods Balay *et al.* (2014); *hypr* (2014).

We note also that the boundary conditions for Eq. (8) are of pure Neumann type (unless e.g. an outlet pressure is specified), which results in a singular matrix. These boundary conditions arise from the projection method and are not physical. The common “engineering” approach of fixing the singularity, simply fixing the pressure at some point in the domain, is not a very good approach as it may pollute the spectrum of the preconditioner. Instead, projecting the discretized singular equation into the orthogonal complement of the null space of the singular matrix seems to be a good solution Zhuang and Sun (2001). In other words, for  $Ax = b$ , we construct the Krylov operator  $K = (\mathbb{I} - \mathbb{N})P^{-1}A$  such that  $b, Kb, K^2b, \dots$  is orthogonal to the null space  $\mathbb{N}$ . Here  $\mathbb{I}$  is the identity matrix, so  $(\mathbb{I} - \mathbb{N})P^{-1}$  is the desired projection. In the PETSc library that we employ here Balay *et al.* (2014), this is achieved using the `KSPSetNullSpace()` routine.

### 4 Parallelization

The starting point for the parallelization was an in-house code consisting of a 2D/3D Navier-Stokes solver and a multi-physics framework that enables the simulation of two-phase flows with the possibility of applying electric fields, and/or adding surface-active agents to the interface. The interface between the two phases is captured using a level-set method, so interfaces with changing topology such as two merging drops can be simulated. The code has been successfully applied to the study of both liquid-liquid Teigen and Munkejord (2010) and liquid-gas systems Ervik *et al.* (2014), but the long runtime has restricted its use to 2D axisymmetric cases so far.

The PETSc DMDA framework for domain decomposition was chosen as the main methodology for parallelizing the code. Domain decomposition consists in splitting the whole domain into subdomains which are each

distributed to one MPI node. Each node then has a computational domain with some internal cells where the flow is computed, and some ghost cells which represent either boundary conditions or values that belong to neighbouring domains. This means that regular communication between the nodes is necessary such that all ghost cells have correct values. Such a splitting is shown in Fig. 2 below. Neglecting for a moment the pressure Poisson equation, this approach can scale well to millions of CPU cores, see e.g. Rossinelli *et al.* (2013) for an example in compressible flow.

By using the PETSc DMDA framework we can avoid the gritty details of domain decomposition and MPI programming. At the initialization of the code, some routines are called to set up three DMDAs which are objects that manage the decomposition. Using these objects we input how large our computational domain should be in terms of grid points, and the library decides an optimal decomposition *at runtime* depending on the number of MPI processes the code is run with. We also specify the physical dimensions of our uniform grid, and the library returns the physical dimensions for each subdomain.

This framework is very convenient, but one enhancement was made to further facilitate the reuse of the serial code. In the standard PETSc framework, the local work arrays that represent the solution on a given subdomain and the values in the ghost cells are indexed using the global indices. The existing code naturally expects indices that go from 1 to the maximum value `imax`. In Fortran, the bounds of an array may be re-mapped when the array is passed to a subroutine, and this feature was used to ensure that each local work array had bounds as expected by the serial code. Thus we will use `imax` as the final `i` index *on each subdomain* in the following.

With this enhancement, the only thing that had to be re-written in the original code was the handling of the staggered grid for the velocity. In the formulation used here, we have one less point for e.g.  $u$  in the  $x$  direction, since these values are located at the cell faces. In the serial code this is handled by not solving for  $u$  at the point `imax`. In the parallel version,  $u$  at the point `imax` should however be solved for on those processes that are not at the actual boundary but where there is a neighbouring process in the positive  $x$ -direction.

Furthermore, this means that a communication step is also necessary in the projection method. After the pressure has been calculated from the Poisson equation, we calculate e.g. the  $x$ -component of  $\nabla p$  at the cell face corresponding to  $u$  at `imax`. Numerically this is  $(p(\text{imax}+1) - p(\text{imax}))/dx$ , so the ghost value at `imax+1` must be updated before this calculation for those subdomains where  $p(\text{imax}+1)$  represents a pressure value on another subdomain and not a boundary condition.

Returning to the pressure Poisson equation Eq. (8), the elliptic nature of this equation means that, in some sense, all nodes must communicate during the solution. A further reduction in speedup potential is due to the fact that the solvers for this equation are mostly bound by memory bandwidth, which is shared amongst all cores on a modern CPU. These limits imply that we must lower our expectations somewhat in comparison with

the impressive results mentioned earlier for compressible flows.

In the DMDA framework, the Poisson equation is set up such that each process computes its own portion of the matrix and right-hand side vector. This is the only scalable way of solving it, even when sparse storage formats are used.

## 5 Results

### 5.1 Manufactured solution case

After the code had been parallelized it was tested using a manufactured solution Roache (2002) inspired by that used in John *et al.* (2006). The debugging tool Valgrind Nethercote and Seward (2007); Nethercote *et al.* (2014) was used in the memory checking mode to ensure that the code does not e.g. make use of uninitialized values, a common programming error. When all such errors were fixed, the code was used to solve the single-phase Navier-Stokes equations with the following exact solution used as an initial – boundary value problem on a  $(1.0 \text{ m})^3$  domain, where the origin is in the lower left front corner (cf. Fig. 2).

$$\begin{aligned} u &= t^3 yz \\ v &= t^2 xz \\ w &= txy \\ p &= x + y + z - 1.5 \end{aligned} \tag{10}$$

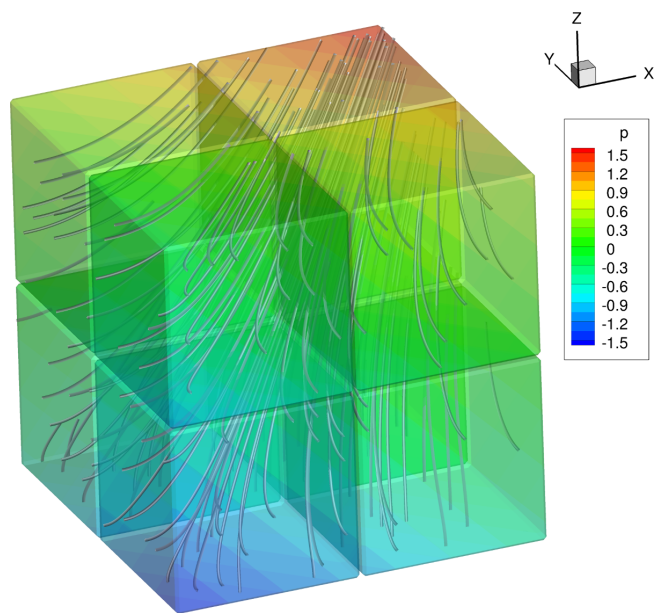


Figure 2: The computed solution after 0.031 s (100 time steps) on a  $128^3$  grid run on 8 processors. The blocks show the decomposition of the domain, the pressure field is shown superimposed on these blocks, and the streamlines illustrate the flow.

Insertion into Eq. (1) confirms that this solution is divergence free, and the resulting body force can be computed by inserting Eq. (10) in Eq. (2). In order to minimize the risk of human error, this was done symbolically using Maple, the resulting expression was

copied into the Fortran code and regular expressions were used to convert Maple syntax into Fortran. A plot of the computed solution is shown in Fig. 2. Here the velocity streamlines are shown together with the pressure field which has been superimposed on blocks representing the parallel decomposition.

## 5.2 Convergence

Using the manufactured solution in Eq. (10), the convergence under grid- and time step refinement, as well as the strong and weak scaling, was tested on the Kongull cluster at NTNU. This cluster has dual-socket nodes with Intel Xeon E5-2670 8-core CPUs and a 1 Gb/s Ethernet interconnect. The STREAM benchmark McCalpin (2014, 1995) was run on one core and gave an effective memory bandwidth of 9800 MB/s for the Triad test<sup>3</sup>.

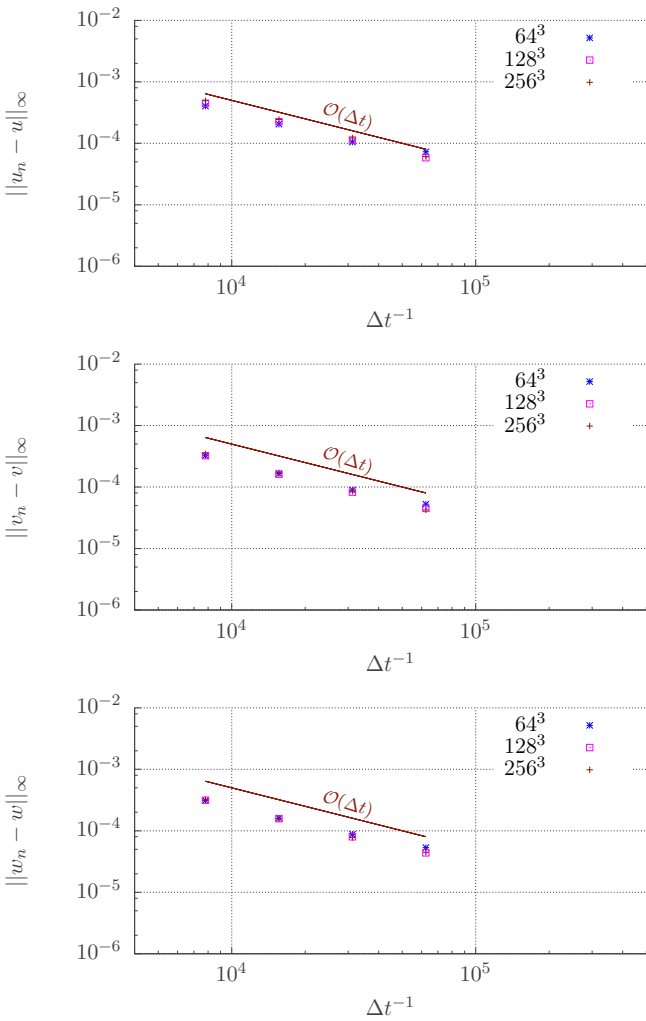


Figure 3: Time step and grid refinement on 32 processes. Top to bottom:  $u$ ,  $v$  and  $w$  velocities. The maximum error of the solution, e.g.  $\|u_n - u\|_\infty$  is plotted against the inverse of the time step. Here  $u_n$  denotes the numerical solution at time step  $n$  while  $u$  denotes the exact solution at this time.

To test the grid- and time step refinement, a base case

<sup>3</sup>The Triad test consists of repeated computations of the operation  $\mathbf{a}(i) = \mathbf{b}(i) + \mathbf{q} * \mathbf{c}(i)$  where  $\mathbf{q}$  is constant and  $i$  is incremented.

was selected with a  $256^3$  grid, giving a grid spacing  $\mathbf{dx}$  of  $3.91 \cdot 10^{-3}$  m, the CFL condition following Kang *et al.* (2000) with a CFL number of 0.5 then giving a time step of  $1.28 \cdot 10^{-4}$  s. This case was solved for 100 time steps, as were solutions on coarser grids  $128^3$  and  $64^3$  computed with the same time step. All simulations were run on 32 processes (8 nodes with 4 processes each). Subsequently, the same cases were run but with 1/2, 1/4 and 1/8 the time step using 200, 400 and 800 time steps, respectively. The results are shown in Fig. 3.

It is seen that the convergence behaviour is as expected. First of all, the temporal order is 1 (not 2) due to an irreducible splitting error from the projection method. This can be overcome e.g. by using the incremental pressure form (see Guermond *et al.* (2006) for a review of projection methods), but has not been considered in this work. Second, the grid refinement does not influence the error. This is due to the fact that the velocity field is linear in space, so the error is completely dominated by the temporal order.

## 5.3 Strong scaling

To test the strong scaling of our code, i.e. how simulating a given case speeds up when more processes are used, a  $128^3$  grid was used giving a grid spacing  $\mathbf{dx}$  of  $7.81 \cdot 10^{-3}$  m, the CFL condition giving a time step of  $3.10 \cdot 10^{-4}$  s. The solution was computed for 100 time steps. Since the Poisson solver performance should be bound by memory bandwidth, the test was made using 2 processes per node (one per socket) and several nodes. The resulting speedup relative to one process is shown in Fig. 4. In this figure, the black points indicate the speedup compared to running on one process. The scaling seen is quite good, but as expected lower than the theoretical linear scaling. It is seen that the peak memory usage (orange) increases slightly with more processes.

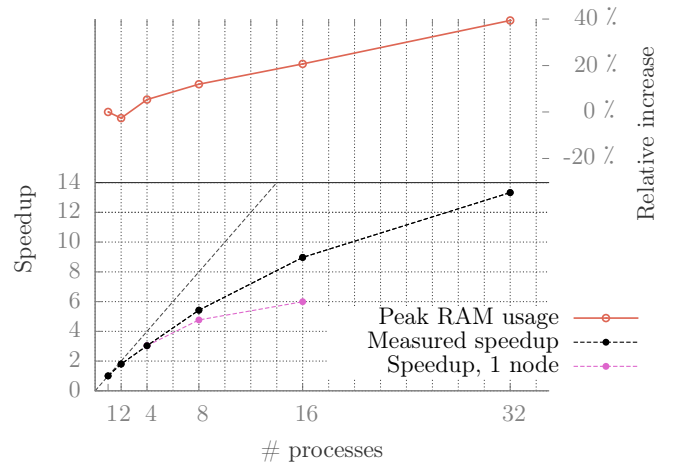


Figure 4: Strong scaling: with the left-hand-side  $y$ -axis, measured (black and magenta) and the optimal (dotted gray) speedup plotted against the number of processes. With the right-hand-side  $y$ -axis, increase in memory use.

To investigate the hypothesis that using only 2 processes per node and several nodes is better than using many processes on one node, we also tried running with

8 and 16 processes on one node. These results are plotted in magenta in Fig. 4 and confirm the hypothesis. We can conclude that even on this particular cluster with a slow (by HPC standards) interconnect, the added memory bandwidth afforded by using more nodes (thus more sockets) outweighs the penalty of increased communication between nodes. This also indicates that the results for 2 processes per node are bound by the interconnect speed, such that the speedup would be closer to the optimal (linear) scaling when run on a more tightly-coupled cluster.

## 5.4 Weak scaling

The weak scaling of the code was also studied. The base case was the same manufactured solution on a  $(0.5 \text{ m})^3$  domain resolved with a  $64^3$  grid, run on one process. Then a  $(0.5 \text{ m})^2 \times (1.0 \text{ m})$  domain with a  $64^2 \times 128$  grid was solved with two processes, a  $(0.5 \text{ m}) \times (1.0 \text{ m})^2$  domain with a  $64 \times 128^2$  grid was solved on 4 processes, etc. In this way, the number of grid points and the number of processes are both increased proportionally. The equations were solved for 50 time steps, and the results are shown in Fig. 5.

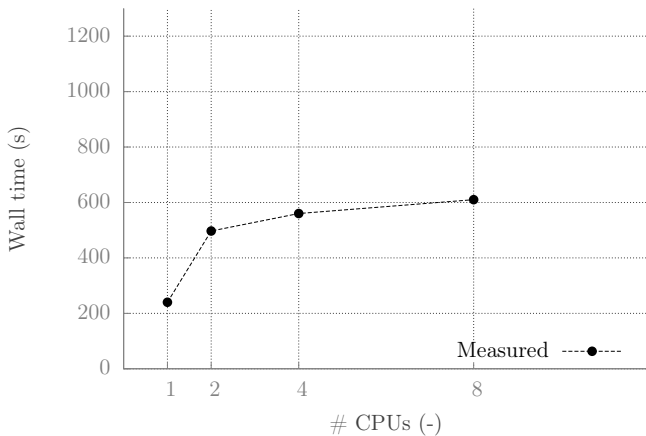


Figure 5: The weak scaling of the code as the number of processes and the number of grid points are both increased proportionally.

As is seen in this figure, there is obviously a performance hit initially; the perfect behaviour would be a flat line. This is as expected. When going from 1 to 2 processes, we go from no communication to overhead from communication. Furthermore, when going from 2 to 4 processes, there is the added overhead of intra-node communication, as opposed to the case with 2 processes where the communication is not over the network but over the CPU bus. The weak scaling seen here is quite decent. One should also be aware that it is more difficult to ensure that cases are “equivalently hard” for weak scaling than for strong scaling Aagaard *et al.* (2013).

## 5.5 Two-phase results

As an initial test of the two-phase capabilities of the parallelized code, the CSF method was employed to simulate a 2 cm diameter drop with properties  $\rho_1 = 2 \text{ kg/m}^3$ ,  $\mu_1 = 0.01 \text{ Pa s}$  falling through a bulk fluid

with properties  $\rho_2 = 1 \text{ kg/m}^3$ ,  $\mu_2 = 0.05 \text{ Pa s}$ . The interfacial tension was set to  $\sigma = 0.01 \text{ N/m}$ . The domain was  $(10 \text{ cm})^3$  resolved by a  $(128)^3$  grid, the simulation was run on 8 processes for 33900 time steps up to  $t = 0.01 \text{ s}$ . The drop has not yet achieved a substantial falling velocity, so the spurious currents are quite visible. The result is shown in Fig. 6, where the drop is shown with the pressure superimposed on the surface, streamlines indicating the flow. A plane is shown intersecting the centre of the drop, on this plane the pressure field, velocity field and level-set function contour lines are shown. A reference vector is shown on the right.

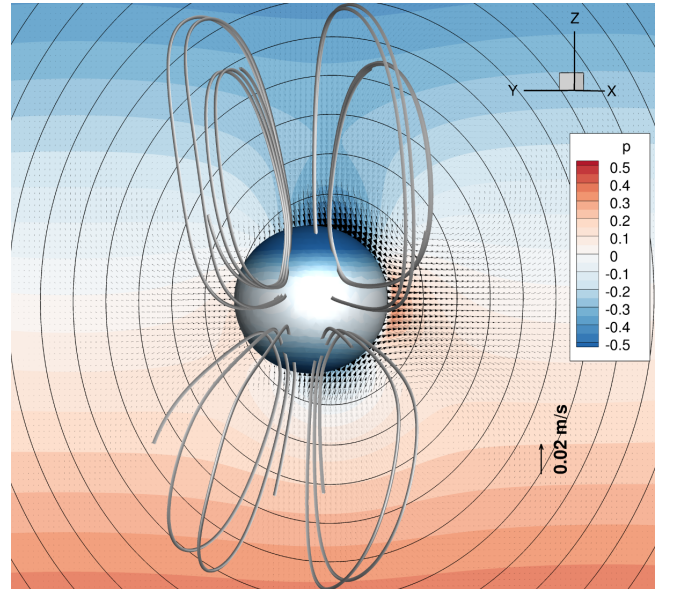


Figure 6: The falling drop after a short time (0.01 s). The pressure field is shown superimposed on the surface, and on the plane behind the drop. On this plane the velocity field and the level-set isocontours are also shown. Streamlines indicate the velocity field.

Spurious currents is a well-known challenge with the CSF method, and experience with the 2D serial code has led us to prefer the ghost-fluid method (GFM) Kang *et al.* (2000), which is somewhat more complicated to implement. This was not done within the scope of this paper. Nevertheless, this demonstrates that the parallel code is capable of two-phase fluid simulations with both density- and viscosity-jumps.

## 6 Conclusions

In this paper we have discussed the parallelization of an existing serial 3D incompressible Navier-Stokes solver for two-phase flow. The PETSc DMDA domain decomposition framework has been leveraged to apply MPI parallelism, enabling the code to make use of modern HPC facilities. We have discussed the alterations that were necessary for the serial code and established a framework where these were as few as possible.

Based on this code, we have reported the strong and weak scalings for a manufactured-solution case on a cluster with dual-socket nodes and 1 Gb/s Ethernet interconnect. It is seen that the code scales rather well, but that one

should take care to maximize the number of sockets used, since the Poisson solver is bound by memory bandwidth. If this code is run on a cluster simultaneously with CPU-bound parallel codes (e.g. using Monte Carlo methods), sensible resource allocation would benefit from taking the available memory bandwidth into account. Then it would not be optimal to allocate all cores on  $N$  nodes to this code, but rather e.g. 50% of the cores on  $2N$  nodes, while a CPU-bound code could effectively utilize the remaining 50% of the cores.

The speedup seen in the strong scaling test (13x faster on 32 processes) is sub-linear but does not level-off. Together with the possibility of running on more tightly-coupled clusters where the behaviour should be closer to linear, and using more than 32 cores, this will give a substantial speedup and reduce the runtimes of weeks and months for the serial code to something more manageable, i.e. a few days or less.

Initial tests demonstrate that the code is able simulate two-phase flow, but the ghost-fluid method (GFM) should be used instead of the CSF method currently employed, in order to minimize the spurious currents.

This effort has left us with a code that scales quite well and a framework where the remaining multi-physics components can easily be introduced. In the end this will enable future simulations of full 3D cases relevant for the fundamental understanding of electrocoalescence.

## 7 Acknowledgement

We would like to thank Matthew Knepley, Barry Smith and Jed Brown of the PETSc project for useful discussions around the framework employed here.

This work was funded by the project *Fundamental understanding of electrocoalescence in heavy crude oils* coordinated by SINTEF Energy Research. The authors acknowledge the support from the Petromaks programme of the Research Council of Norway (206976), Petrobras, Statoil and Wårtsilä Oil & Gas Systems.

## References

- AAGAARD, B.T. *et al.* (2013). “A domain decomposition approach to implementing fault slip in finite-element models of quasi-static and dynamic crustal deformation”. *J. Geophys. Res.: Solid Earth*, **118**(6), 3059–3079.
- BALAY, S. *et al.* (2014). “PETSc Web page”. <http://www.mcs.anl.gov/petsc>.
- BRACKBILL, J. *et al.* (1992). “A continuum method for modeling surface tension”. *J. Comput. Phys.*, **100**(2), 335–354.
- CHORIN, A.J. (1968). “Numerical solution of the Navier-Stokes equations”. *Math. Comput.*, **22**(104), 745–762.
- DUFFY, A. *et al.* (2002). “An improved variable density pressure projection solver for adaptive meshes”. Unpublished. See <http://www.math.fsu.edu/~sussman/MGAMR.pdf>.
- ERVIK, Å. *et al.* (2014). “A robust method for calculating interface curvature and normal vectors using an extracted local level set”. *J. Comput. Phys.*, **257**, 259–277.
- GOTTLIEB, S. *et al.* (2009). “High order strong stability preserving time discretizations”. *J. Sci. Comput.*, **38**(3), 251–289.
- GUERMOND, J. *et al.* (2006). “An overview of projection methods for incompressible flows”. *Comp. Meth. Appl. Mech. Eng.*, **195**(44), 6011–6045.
- HENSON, V.E. and YANG, U.M. (2000). “BoomerAMG: a parallel algebraic multigrid solver and preconditioner”. *Appl. Numer. Math.*, **41**, 155–177.
- hypre (2014). *High Performance Preconditioners*. Lawrence Livermore National Laboratory. <http://www.llnl.gov/CASC/hypre/>.
- JOHN, V. *et al.* (2006). “A comparison of time-discretization/linearization approaches for the incompressible Navier–Stokes equations”. *Comput. Meth. Appl. Mech. Eng.*, **195**(44), 5995–6010.
- KANG, M. *et al.* (2000). “A boundary condition capturing method for multiphase incompressible flow”. *J. Sci. Comput.*, **15**(3), 323–360.
- LIU, X.D. *et al.* (1994). “Weighted essentially non-oscillatory schemes”. *J. Comput. Phys.*, **115**(1), 200–212.
- MCCALPIN, J.D. (1995). “Memory bandwidth and machine balance in current high performance computers”. *IEEE Computer Society Technical Committee on Computer Architecture (TCCA) Newsletter*, 19–25.
- MCCALPIN, J.D. (2014). “STREAM web site”. <http://www.cs.virginia.edu/stream/>.
- MOORE, G. (1965). “Cramming more components onto integrated circuits”. *Electronics*, **38**(8).
- NETHERCOTE, N. and SEWARD, J. (2007). “Valgrind: a framework for heavyweight dynamic binary instrumentation”. *ACM Sigplan Notices*, vol. 42, 89–100.
- NETHERCOTE, N. *et al.* (2014). “Valgrind Web page”. <http://valgrind.org/>.
- OSHER, S. and FEDKIW, R.P. (2001). “Level set methods: An overview and some recent results”. *J. Comput. Phys.*, **169**(2), 463 – 502.
- OSHER, S. and FEDKIW, R.P. (2003). *Level Set Methods and Dynamic Implicit Surfaces*. Springer, Berlin.
- OSHER, S. and SETHIAN, J.A. (1988). “Fronts propagating with curvature-dependent speed: Algorithms based on Hamilton–Jacobi formulations”. *J. Comput. Phys.*, **79**(1), 12 – 49.

- ROACHE, P.J. (2002). “Code verification™ by the method of manufactured solutions”. *ASME J. Fluids Eng.*, **124(1)**, 4–10.
- ROSSINELLI, D. *et al.* (2013). “11 PFLOP/s simulations of cloud cavitation collapse”. *SC*, 3.
- TEIGEN, K.E. and MUNKEJORD, S.T. (2010). “Influence of surfactant on drop deformation in an electric field”. *Phys. Fluids*, **22(11)**. Article 112104.
- VAN DER VORST, H. (1992). “Bi-CGSTAB: A fast and smoothly converging variant of Bi-CG for the solution of nonsymmetric linear systems”. *SIAM J. Sci. Comput.*, **13(2)**, 631–644.
- ZHUANG, Y. and SUN, X.H. (2001). “A high-order fast direct solver for singular Poisson equations”. *J. Comput. Phys.*, **171(1)**, 79 – 94.